

Manuscript version: Author's Accepted Manuscript

The version presented in WRAP is the author's accepted manuscript and may differ from the published version or Version of Record.

Persistent WRAP URL:

<http://wrap.warwick.ac.uk/171656>

How to cite:

Please refer to published version for the most recent bibliographic citation information. If a published version is known of, the repository item page linked to above, will contain details on accessing it.

Copyright and reuse:

The Warwick Research Archive Portal (WRAP) makes this work by researchers of the University of Warwick available open access under the following conditions.

© 2022, Elsevier. Licensed under the Creative Commons Attribution-NonCommercial-NoDerivatives 4.0 International <http://creativecommons.org/licenses/by-nc-nd/4.0/>.



Publisher's statement:

Please refer to the repository item page, publisher's statement section, for further information.

For more information, please contact the WRAP Team at: wrap@warwick.ac.uk.

Accelerated State of Health Estimation of Second life Lithium-ion Batteries via Electrochemical Impedance Spectroscopy Tests and Machine Learning Techniques

Mona Faraji-Niri ^{a,*}, Muhammad Rashid ^a, Jonathan Sansom ^a, Muhammad Sheikh ^{a,b}, Dhammika Widanage ^a, James Marco ^a

^aWMG, University of Warwick, Gibbet Hill Road, Coventry, CV4 7AL, UK

^bSchool of Digital, Technologies and Arts, Staffordshire University, College Road, University Quarter, Stoke-on-Trent, ST4 2DE, UK

*mona.faraji-niri@warwick.ac.uk

Abstract

Estimating the State of health (SoH) of Lithium-ion (Li-ion) batteries is a challenging task due to cross coupling and dependency between ageing mechanisms. An accurate estimation is particularly essential for second-life batteries to facilitate their successful implementation in the new application. By adopting the Electrochemical Impedance Spectroscopy (EIS) test and a machine learning (ML) approach, the accelerated SoH estimation problem is studied here. For this purpose, 325 experiments for 30 Li-ion cells were conducted at various SoH, temperature, and state of charge. First an optimised Gaussian Process Regression model is developed and validated for SoH estimation. Then the sensitivity of the model is evaluated relative to measurement noise. Finally, the model's robustness is quantified through a case study involving cells that have been characterised with different physical test equipment. The results demonstrate that the model can predict the SoH of Li-ion cells with an error about 1.1% and is reasonably robust to the various testing conditions of the battery. The methodology for handling the EIS data within a machine learning framework, the sensitivity analysis and the robustness quantification techniques are the main novelties of this study in the context of grading Li-ion batteries for second-life applications

Keywords: Electrochemical Impedance spectroscopy, Second life Lithium-ion batteries, Machine Learning, State of health, Prediction

I. Introduction

With the drastic increase in the number of hybrid and electric vehicles (EVs) in recent years, the global demand for lithium-ion batteries as their main power source has gone up significantly. This demand is expected to grow by 26% from 2021 to 2031, with a market value of about \$70 billion by 2026 [1]. This record-breaking demand and the high production cost of lithium-ion batteries have attracted attentions toward the reuse, recycle and disposal management of those soon after they are technically at their end of life (EoL) in the EVs [2].

Reusing the batteries has significant economic benefits and reduced environmental impacts. In the case of lithium-ion batteries for EVs, the remaining energy capacity of cells has a direct impact on the vehicles remaining range and its safety. Generally, when the cell's state of health (SoH), which is the ratio of the present capacity to the initial capacity [3, 4], falls below 80%, it is considered retired due to reduced ability of supplying the energy and power for the EVs [5]. The retired batteries while not of any use for EVs can still be repurposed and utilised in many other applications, in fact they play an important role in energy storage systems that require relatively lower energy or power. Examples of such applications include load-shifting and frequency regulation in grid-scale [6, 7]. A comprehensive review of the applications of second-life batteries can be found in [5].

43 An accurate estimation of SoH is necessary for its safe and reliable implementation in the next life
44 application. There exist several techniques to test retired batteries. In [8], constant current pulses are
45 utilised to evaluate the cycle life of cells. Electrochemical models are developed by [9, 10] to capture
46 the ageing mechanism of batteries by quantifying the change in the volume of the cyclable lithium-
47 ions as well as the solid electrolyte interphase film resistance [11]. These electrochemical models are
48 hard to be derived for second-life cells as their parametrisation is much more challenging, due to
49 complex and nonlinear grading mechanisms, compared to the new cells. In search for methods with
50 affordable cost and complexity for SoH estimation, a few studies have focused on the identification of
51 certain parameters of cells as health indicators. Admitting that the cell energy capacity is a measure
52 of its health, techniques based on incremental capacity and differential voltage are very common in
53 this category [12, 13]. Beside energy capacity, the battery impedance can also serve as an indicator
54 for its SoH, several researchers have focused on impedance measurement via an electrochemical
55 impedance spectroscopy (EIS) test [14, 15]. EIS test determines the battery impedance at different
56 frequencies and is considered as one of the off-line, non-intrusive and in-situ techniques for SoH
57 characterisation [15]. It is favourable as only requires voltage and current measurements in the
58 frequency domain.

59 EIS measurements have been used for SoH estimation of cells in a few studies of different applications.
60 In [16] 3-electrode pouch cells were tested via EIS and modelled via equivalent circuits with a SoH
61 estimation accuracy of 7%. An estimation of the Li-ion battery cell SoH during its operation is proposed
62 in [17] by designing an EIS test for measuring the cell impedances at different SoC, and temperatures.
63 Quasi-EIS tests are conducted in [18], and an empirical method with an error up to 1% is utilised in
64 [19] to estimate the battery SoH considering its relaxation time. An identification of different ageing
65 mechanisms addressing active material loss and loss of lithium-ions is performed in [20]. An online or
66 so called in-operando version of the EIS test for the SoH estimation of cells is proposed in [21].

67 Most of the abovementioned studies have focused on just one or only on a handful number of cells,
68 which makes generalisation of the algorithms to real-world problems quite challenging. Considering
69 the high volume of data points and the information generated via energy capacity or impedance
70 determination tests, data driven approaches such as machine learning (ML) are very suitable to
71 perform SoH estimation on a large stack of cells. SoH estimation based on ML models has been
72 recently addressed in a few studies. For example, an ensemble model based on usual capacity test
73 data is developed in [22] for predicting the remaining useful life of the cells. The model is an infusion
74 of an empirical and a polynomial regression model tested on six individual cells at room temperature.
75 Extreme learning models are developed in [23, 24] for degradation estimation of cells tested under
76 specific loading profiles and real-world cycling conditions [25]. Deep learning models based on
77 capacity tests are proposed in [26] for SoH prognostics of connected cells in a series configuration. A
78 combination of linear and Gaussian support vector machines is developed in [27] to improve the cycle
79 life prediction. Long short-term memory models based on the capacity tests are developed in [28, 29]
80 and tested on experimental and open-source data set with a SoH error estimation error below 1.46%.

81 Focusing on EIS test, while they can be very useful for SoH characterisation of cells in larger volumes,
82 they have not yet been fully investigated with this aim. Example researches include EIS measurements
83 combined with fuzzy logic algorithms for SoH characterisation of cells as addressed in [30, 31] and
84 regression models based on twelve Li-ion cells EIS spectrum developed in [32]. A comprehensive study
85 based on the EIS field data for the online estimation of SoH is performed in [33] where the degradation
86 is monitored at the electrode level. A neural network based on EIS tests and equivalent circuit analysis
87 is developed in [34] with the predictions of equivalent series resistance, charge-transfer resistance,
88 and solid-electrolyte interphase resistance as representation of cells state of health by errors below

89 5%, 1.5%, and 1%, respectively. The zero-crossing frequency of the li-ion cells is considered as a feature
90 to train a neural network for SoH estimation in [35]. A study based on EIS measurements at constant
91 temperatures is performed via Gaussian process regression models for the estimation of remaining
92 useful life of commercial cells for up to 300 cycles in [36].

93 While there are relatively large number of methods developed for SoC estimation via EIS tests and
94 machine learning approaches [37, 38], not enough attention has been given to the SoH estimation by
95 EIS experiments and there is an obvious research gap specially for second life battery applications.
96 One of the main differences between the new and re-purposed cells is the inconsistency in between
97 their characteristics [2, 39]. This inconsistency and difference between the cells usually lead to
98 different ageing patterns and SoH for the cells. Therefore, tailoring the SoH estimation algorithms and
99 methods for larger number of cells at their second life is still required. To address this issue and take
100 the advantage of EIS measurements, this study focuses on the SoH estimation of NMC cells via EIS
101 tests and a machine learning modelling approach. This research answers the following questions:

- 102 1. If the EIS test data can be directly used for the SoH estimation of cells or feature engineering
103 is necessary?
- 104 2. What is the configuration of a ML model for SoH estimation?
- 105 3. How robust the method is to the measurement noise?
- 106 4. How generalisable are the ML-based models to real-world uncertainties arising from
107 variations in test equipment?
- 108 5. What is the minimum amount of conditioning information required for an accurate SoH
109 estimation?

110 To answer the above questions, first a series of EIS characterisation tests are conducted to provide
111 training and validation data for the study. To factor in the impact of the cell-to-cell variation and
112 facilitating an analysis based on the similarities and differences between the cells during the SoH
113 estimation, each test is conducted on 4 batteries of the same type and from the same manufacturer.
114 To uncover the impact of the testing temperature and the state of charge on the cells SoH
115 predictability, the tests are run at three different temperatures of 15, 25, and 35 °C as well as 5
116 different SoC breakpoints between 5% to 95% (5, 20, 50, 70, 95). The correlation in between cell
117 impedance, SoC, temperature and its SoH is built via a machine learning model. In this context, a
118 Gaussian Process Regression model is developed and optimised via Bayesian methods. The model is
119 created for two scenarios to identify the minimum amount of information for an accurate estimation
120 and the necessity of feature engineering. In the first scenario, the full EIS data and in the second one,
121 the selected features are utilised for building the ML model. For the first time in this study, a
122 methodology is proposed to evaluate the model's sensitivity to the measurement noise by generating
123 synthetic noisy inputs for the model. Additionally, the model's robustness is evaluated under a testing
124 condition with different experimental equipment and cooling mechanism as well as the different set
125 of model inputs for studying its generalisability. A brief diagram of this paper's proposal is as [Figure 1](#).

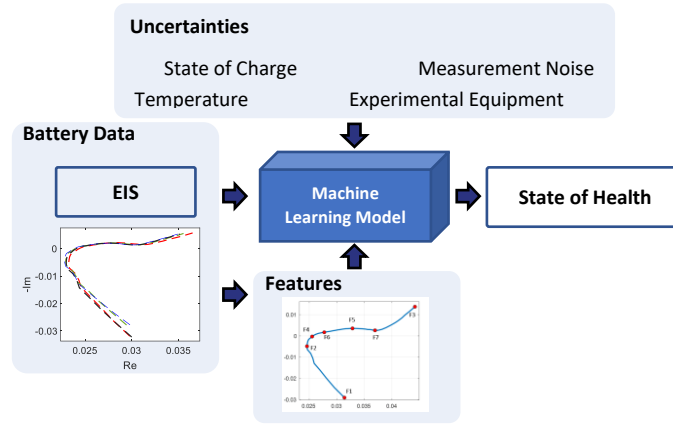


Figure 1: The diagram of the machine learning model for the prediction of the cell SoH via EIS test

The remainder of this paper is as follows, Section II, give the experimental details, the test protocols, and the plans. Section III articulates the machine learning modelling approach. In this section, the list of inputs and outputs, the definition of features and their extraction process is also given. Section VI includes the main results related to the prediction of the SoH. Section V includes discussions regarding the sensitivity and robustness of models. The final section summarises the methodology, results and findings and concludes the paper.

II. Experiments

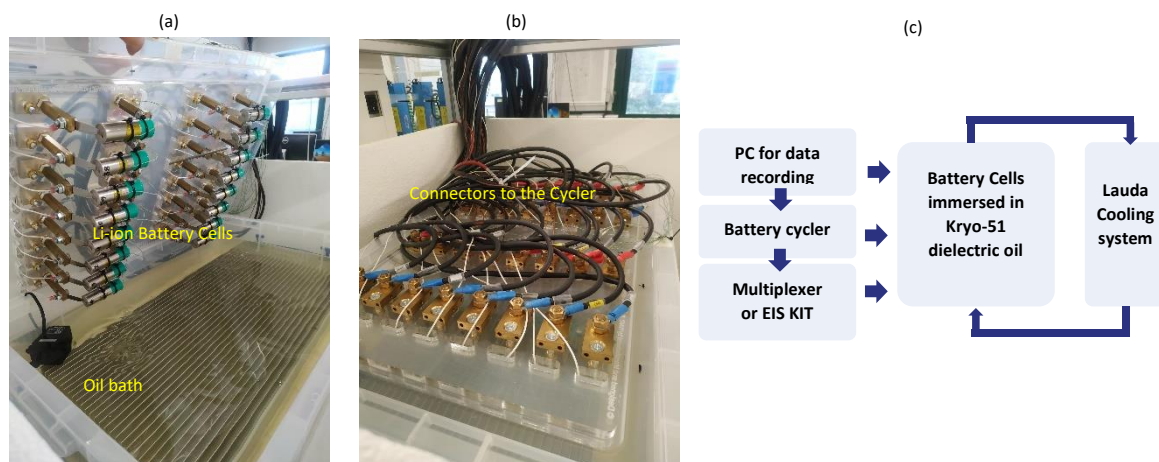
To conduct this study, 30 Lithium-ion commercial LGM50 cells with NMC chemistry have been utilised. The rated capacity of cells was 5 Ah defined by the manufacturer. The initial capacity of all the cells has been measured as the reference for their state of health at C/3 current charge-discharge between 4.2 V to 2.5 V with a C/20 cutoff current at constant voltage mode during charge at 25 °C. Based on the reference capacity, the cell's state of health has been defined via Eq (1).

$$SoH(\%) = \frac{Current\ Capacity(Ah)}{Reference\ Capacity(Ah)} \times 100 \quad (1)$$

From the initial 30 cells, subsets of cells have been aged to produce 4 additional case breaks of 80, 85, 90 and 95% SoH where it has been assumed that the reference case is related to the 100% SoH. For each SoH subset in addition to the 1st cell tested 4 further cells have been aged similarly and stored under similar conditions, where their performance has been examined subsequently. This was required to evaluate cell-to-cell variation during analysis. The cycling test for aging was performed using a 10 A Digatron battery cycler with 192 channels where the cells were maintained at 25 °C within a thermal chamber (Binder™). During the cycling process the cells have been charged at C/2 constant-current mode until 4.2 V followed by a constant voltage charge mode until the current drops to C/20 and finished with a discharge at 1C constant current until the cell voltage reaches to 2.5 V. the charge and discharge process has been repeated till the cell reaches the required SoH. For different SoHs, the number of cycles has been different and varying between 60 cycles to reach a 95% SoH and 250 cycles to reach the 80% SoH.

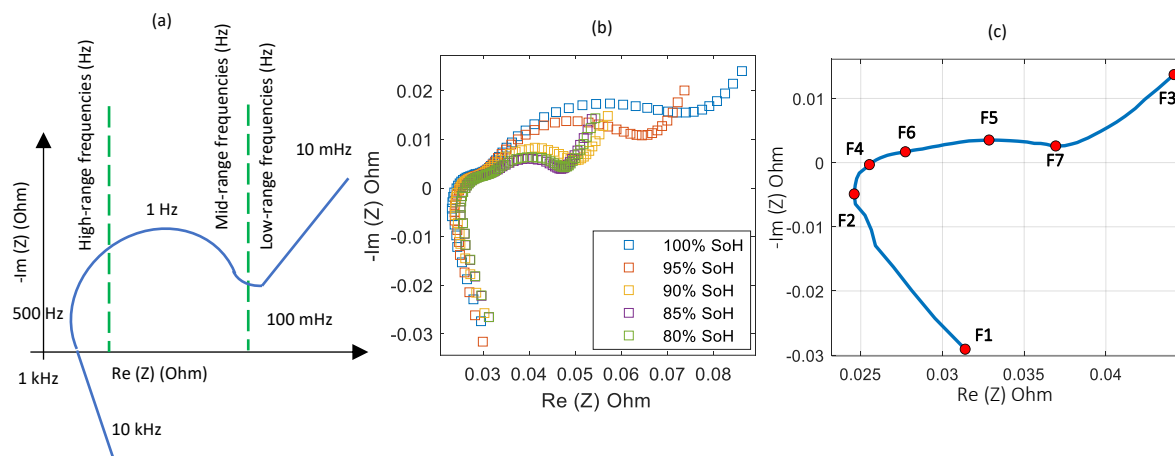
The current capacity of the cells has been quantified for Eq. (1) via a C/3 charge discharge test profile, similar to the reference capacity test case for consistency. After the ageing process, the cells have been subject to a performance test. This comprises the impedance measurement via EIS test at different SoCs (5, 20, 50, 70 and 95%) and temperatures (15, 25 and 35 °C). Before starting the tests, all the cells have been immersed in an oil bath (Kryo-51 dielectric oil) for about 4 hours to guarantee

157 a thermal homogeneity within the cells and across their surface, a Lauda cooling system has been used
 158 to keep the cell's temperature at the defined condition. Figure 2 (a) and (b) show the test and the
 159 experimental setup configuration.



160
 161 **Figure 2:** (a) Battery test setup configuration, (b) Test rig after immersion in oil, (c) Block diagram of the test
 162 setup

163 In performance tests, the cells have been discharged to the desired SoC (using a Coulomb counting
 164 method) at C/3 current and relaxed for 4 hours to minimize the potential/concentration gradients
 165 across the electrode/cell domain caused by the applied current [40, 41]. Once the cell voltage has
 166 reached equilibrium, the EIS measurement is conducted via the Multiplexer equipment in Figure 2 (c)
 167 configuration, between frequencies of 10kHz to 10mHz with a sinusoidal current superimposed on a
 168 DC current at 250 mA. An example EIS Nyquist spectrum is given in Figure 3 (a), where the horizontal
 169 axis refers to the real part of the impedance and the vertical one is for the imaginary part. It is
 170 noteworthy that the frequency values defined in Figure 3 (a) are approximate and the values for a
 171 given cell are known to vary depending on the cell manufacturers, electrochemistry, and form-factor.



172
 173 **Figure 3:** (a) An example EIS spectrum of the Lithium-ion battery, (b) visualisation of some EIS graphs at various
 174 SoH, (c) the feature definition for EIS graphs

175 For each cell, the impedance (Ohm), $Z(f)$ is quantified via Eq. (2), where I and V refer to the sinusoidal
 176 current and voltage at a particular frequency f (Hz). Here, ϕ refers to the phase angle of the voltage.

$$\begin{aligned}
dI &= I_{\max} \sin(2\pi ft) \\
dV &= V_{\max} \sin(2\pi ft + \phi) \\
Z(f) &= \frac{V_{\max}}{I_{\max}} e^{j\phi}
\end{aligned} \tag{2}$$

177 The EIS curve is a good representative of the cell's characteristics, the low frequency section (10 - 100
178 mHz) is associated with the diffusion processes that take place inside the cell, while the medium
179 frequency range (circa 1 Hz) is indicating its double-layer capacitance effect. In the high frequency
180 range (greater than 500 Hz), the interception between the curve and the real axis indicates the cell's
181 Ohmic resistance [37].

182 Following these experiments, a combination of the 30 cells at 5 different SoH, 5 different SoC and 3
183 temperatures have led to 300 cases for the modelling and analysis purposes. Example records of data
184 are visualised on Figure 3 (b) at various SoH, 15 °C and 5% SoC.

185 III. Machine Learning Model

186 To uncover the relation between the EIS measurements of the cells and the associated SoH, the GPR
187 model is created. For this purpose, first the fundamentals of the GPR are given and then the accuracy
188 metrics are provided to evaluate the performance of the model for completeness.

189 GPR is a Bayesian method based on Gaussian processes for non-parametric regression. GPR is deemed
190 to be suitable for dealing with small data set and is capable of providing uncertainty measurements
191 on the predictions [42]. As a Bayesian method, it helps inferring the probability distribution of the
192 parameters in a function that is meant to be learnt through the training process. For a given input
193 indicated by x , the GPR creates a probability distribution function of $f(x)$ with the mean and covariance
194 function of $m(x)$ and $C(x, x')$ as Eq. (3).

$$\begin{aligned}
f(x) &\sim GPR(m(x), C(x, x')) \\
m(x) &= E(f(x)) \\
C(x, x') &= E[(m(x) - f(x))(m(x') - f(x'))]
\end{aligned} \tag{3}$$

195 Here, E is the expected value. $C(x, x')$ is alternatively called a kernel function to capture the relevance
196 between the real responses and predicted values by the similarities of the associated inputs.

197 In the regression process, the prior distribution of the output is specified as Eq. (4), where D refers to
198 the distribution function and its mean value is set to zero for simplicity during the computations.

$$y \sim D(0, C(x, x')) \tag{4}$$

199 Considering y' as the predicted output, x as the training and x' as the test dataset, the joint prior
200 distribution of y' and y is specified by Eq. (5) assuming that the training and test data have the same
201 Gaussian distribution.

$$\begin{pmatrix} y \\ y' \end{pmatrix} \sim D\left(0, \begin{bmatrix} C(x, x) & C(x, x') \\ C(x, x')^T & C(x', x') \end{bmatrix}\right) \tag{5}$$

202 These kernel functions of the GPR need to be carefully selected and their hyperparameters, which are
203 denoted by θ_G , are required to be optimised to guarantee a desirable performance of the model. A
204 review of various kernel functions, their details and hyperparameters is given in [43].

205 The hyperparameter optimisation is usually performed through minimising the negative logarithmic
 206 likelihood function $L(\theta_G)$ given as Eq. (6) using the gradient descent or heuristic approaches [44, 45].

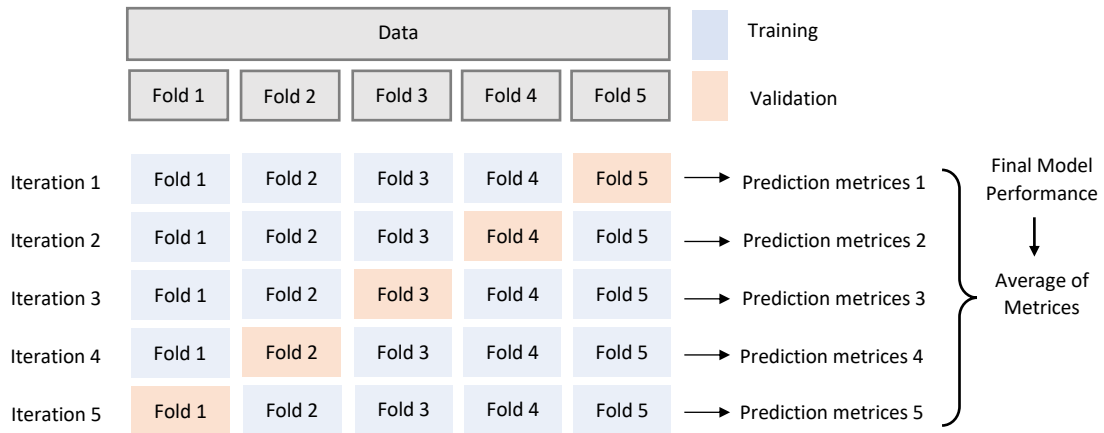
$$L(\theta_G) = \frac{1}{2} \log[\det C(\theta_G)] + \frac{1}{2} y^T C^{-1}(\theta_G) y + \frac{n}{2} \log(2\pi) \quad (6)$$

207 Through this optimisation the predicted output of the test dataset can be obtained through its
 208 conditional distribution by Eq. (7),

$$p(y' | x, y, x') \sim N(y' | \bar{y}', \text{cov}(y')) \quad (7)$$

209 where \bar{y}' is the mean value of the predicted outputs and the $\text{cov}(y')$ is their variance defined by
 210 $\bar{y}' = C(x, x')^T [k(x, x)]^{-1} y$ and $\text{cov}(y') = C(x', x') - C(x, x')^T [k(x, x)]^{-1} k(x, x')$ respectively.

211 To validate the model, the cross-validation (CV) approach is taken [46]. Cross validation is a technique
 212 based on splitting data randomly into K folds and using those folds for training and validation
 213 iteratively. The folds are mutually exclusive portions of the whole dataset, and the idea is to use each
 214 portion at least once for validation. The number of folds is defined by the researcher and the folds
 215 usually have the same size. The diagram of Figure 4 shows the split of the data into $K = 5$ folds of
 216 training and validation. As the figure shows, at each iteration, $K-1$ folds are used for training the model
 217 and the remaining fold is used for validation. CV is very suitable for small to medium size datasets
 218 where there is limited data for validation. The performance of the model is only evaluated based on
 219 the accuracy metrics applied to the validation portion of the data.



220

221 *Figure 4: Cross validation approach for training and evaluating the model performance during validation*

222 To evaluate the performance of the models for the prediction of the SoH values, four complimentary
 223 performance metrics are utilised.

224 Root mean squared error (RMSE), is the first measure which is calculated by Eq. (8) and indicates the
 225 difference between the predicted and real SoH values. Here N is referring to the number of data
 226 points. RMSE has the same unit of SoH so it is in %. Mean squared error (MSE) is the second metric
 227 which is the second power of the RMSE.

$$RMSE = \sqrt{\frac{1}{N} \sum_{j=1}^N (y_j - \hat{y}_j)^2} \quad (8)$$

228 The third metric is R-Squared (R^2), obtained by Eq. (9)

$$R^2 = 1 - \frac{SSE}{TSE} \quad (9)$$

$$SSE = \sum_{j=1}^N (y_j - \hat{y}_j)^2$$

$$TSE = \sum_{j=1}^N (y_j - \bar{y})^2$$

229 where SSE is the sum of the squared error and TSE is the total sum of squares obtained for the
 230 average of all output values $\bar{y} = \frac{1}{N} \sum_{j=1}^N y_j$ for $j = 1, \dots, N$. R^2 is a value between 0 and 1, it does not have
 231 a unit and so reported here in percent. An R^2 of 100% means a perfect prediction where the modelled
 232 outputs and the real values are matched exactly. The final metric is the mean absolute error (MAE)
 233 which is given by Eq. (10).

$$MAE = \frac{1}{N} \sum_{j=1}^N |y_j - \hat{y}_j| \quad (10)$$

234 The four metrics are only applied to the validation portion of the data during each iteration of cross-
 235 validation.

236 IV. Main Results

237 To analyse the performance of the GPR model for the prediction of SoH, two case studies are reported
 238 here. One with all the data points of the EIS graphs as inputs to the model beside the SoC and
 239 temperature, and the other one, with specific features extracted from the EIS graphs as inputs. [Figure 3 \(c\)](#)
 240 shows the approximate features on a sample EIS graph. The list of the inputs for each of the case
 241 studies has been given in the [Table 1](#).

242 *Table 1: The input and outputs for the two case study models based on EIS and conditioning data*

Model	Case Study 1	Type	Case Study 2	Type
Inputs	EIS at 61 frequencies Temperature SoC	Real Imaginary	F1: Highest Frequency point F2: Minimum Real Value point F3: lowest frequency point F4: Zero crossing point F5: Peak point F6: local minima between F4 and F5 F7: local minima between F5 and F3 Temperature SoC	Real Imaginary Frequency
Response	SoH (100% to 80%)		SoH (100% to 80%)	

243 It is worth mentioning that one means to exploit the EIS data to train the ML algorithm is to extract
 244 key features from the spectrum that can be used to characterise the general shape of the EIS response
 245 and the ageing state of the battery. This has the potential advantage of reducing the volume of data
 246 that must be stored to underpin model training and validation. Here, the features are selected
 247 considering the variations in between the cells at different SoHs as well as the expert's view
 248 considering the fact that each of those is a representative of various characteristics of a cell's health
 249 as:

- 250 - F1 is related to the information of cell at the highest frequency
- 251 - F2 is a numerical choice
- 252 - F3 is related to the information of cell at lowest frequency, the slope of the line between F7 and F3
- 253 is related to the gradient of the Warburg impedance

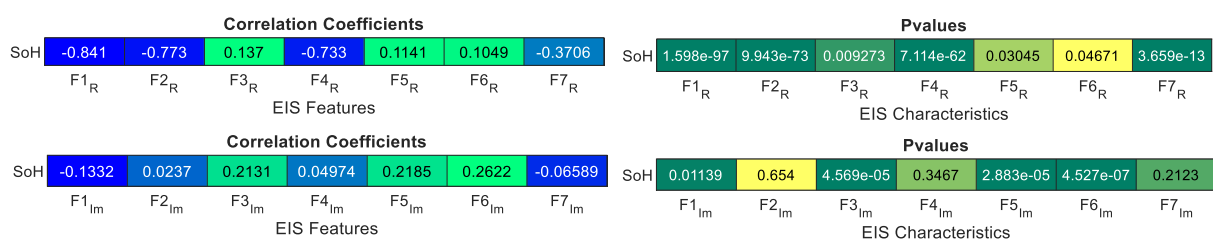
- 254 - F4 is zero-crossing point and related to the DC resistance of cell
- 255 - F6 is related to the possibility of the build-up of formation of the solid electrode interphase layer
- 256 - F5 is related to the value of change transfer impedance
- 257 - F7 is the “turning-point” that represents the transition to diffusion

258 A detailed discussion on each of these factors is beyond the scope of this paper and can be found in a
 259 number of educational texts [47] and research articles highlighting how to interpret the EIS profile of
 260 the lithium-ion battery [48], build an equivalent circuit model of the battery for voltage prediction and
 261 to facilitate control algorithm design [49] and finally to infer battery ageing and the different
 262 degradation modes that impact battery life and performance [48].

263 In order to show the importance and relevance of the selected features of the second case study, a
 264 correlation analysis is performed here. For this purpose the correlation coefficients and their
 265 significance is calculated via Pearson product-moment correlation analysis method [51]. considering
 266 the features as variable F, and the SoH for each case, the coefficients of $r_{F,SoH}$ are obtained via equation
 267 (11). Where, μ is the mean value of each feature, σ is the standard deviation and \mathbb{E} refers to the
 268 expectation.

$$r_{F,SoH} = \frac{\mathbb{E}[(F - \mu_F)(SoH - \mu_{SoH})]}{\sigma_F \sigma_{SoH}} \quad (11)$$

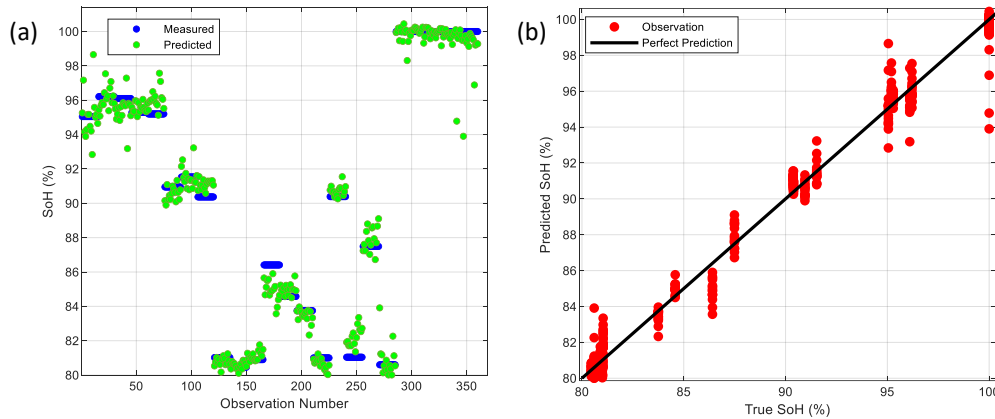
269 The coefficients are values between zero and one and could be positive or negative which refer to
 270 direct or inverse correlation. The closer the value to the one, the stronger the correlation. To be able
 271 to investigate if the correlation between each feature and SoH is demonstrating a significant relation
 272 and the analysis are generalisable from the samples to the population [50] a p-value is also calculated
 273 which denotes the probability of a ‘Null Hypothesis’. The null hypothesis is that there exists no
 274 relationship between the features and the SoH [51]. P-value is a number between zero and one and if
 275 are smaller than a threshold, here 0.1, then the correlation is considered significant. This means the
 276 results are valid in 90% of cases. It is worth to mention that this threshold is a common choice for most
 277 of the data analysis problem. Figure 5 shows the correlation coefficient and p-values of each feature
 278 in relation the cells’ SoH.



279
 280 *Figure 5: Correlation between EIS features and SoH of cells*

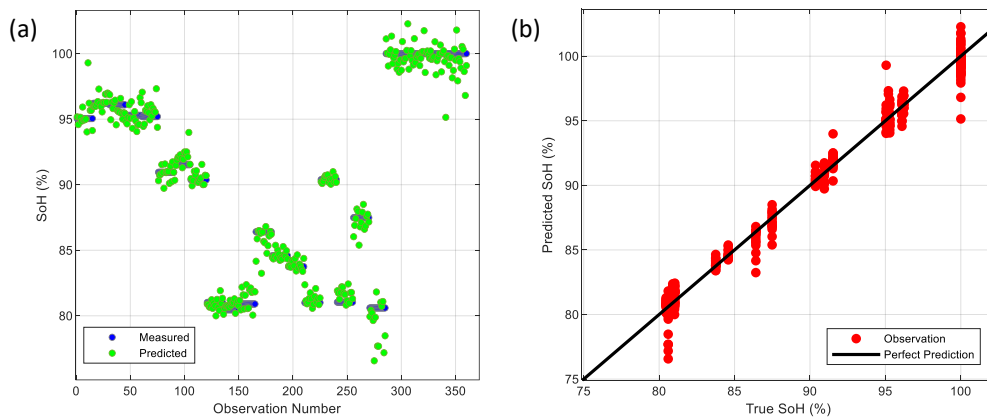
281 As Figure 5 shows, the real part of all features is highly correlated with the SoH of cells, this is
 282 concluded by the correlation coefficients and the p values smaller than the mentioned threshold. It is
 283 worth to highlight that some correlations are direct, and some are inverse and the correlation of the
 284 real part of feature 6 is slightly weaker than others as its lower correlation coefficient shows. Similarly,
 285 the imaginary part of the features is significantly correlated with the SoH value, the weakest
 286 correlation is for the imaginary part of feature 2. Considering this correlation analysis in total all the 7
 287 features could be valuable for the SoH estimation of cell, therefore all of them are considered for the
 288 modelling purposes in what follows.

289 For case study 1, the whole EIS data at various conditions are used for the model and as the frequency
 290 of the measurements has been the same for all cases, it is not a feature for the model. Figure 6 shows
 291 the regression results. Figure 6 (a) is the distribution of predicted and observed data with the record
 292 number, while Figure 6 (b) is showing the positioning of predictions and observations compared to a
 293 perfect prediction.



294
 295 *Figure 6: Regression results for case study 1, (a) predicted and observations SoH value distribution, (b)*
 296 *Predicted and true SoH values against perfect prediction, case study 1*

297 As Figure 6 shows that most of the observations agree with the predicted values from the GPR model.
 298 For case study 2, the regression results are given in Figure 7.



299
 300 *Figure 7: Regression results for case study 2, (a) predicted and observations SoH value distribution, (b)*
 301 *Predicted and true SoH values against perfect prediction, case study 2*

302 Accuracy metrics of both models are listed in Table 2, the results are the mean and standard deviation
 303 (std) of multiple runs to facilitate a more comprehensive conclusion. Here the model has been iterated
 304 for 40 times as a compromise between run time and the stability of the results.

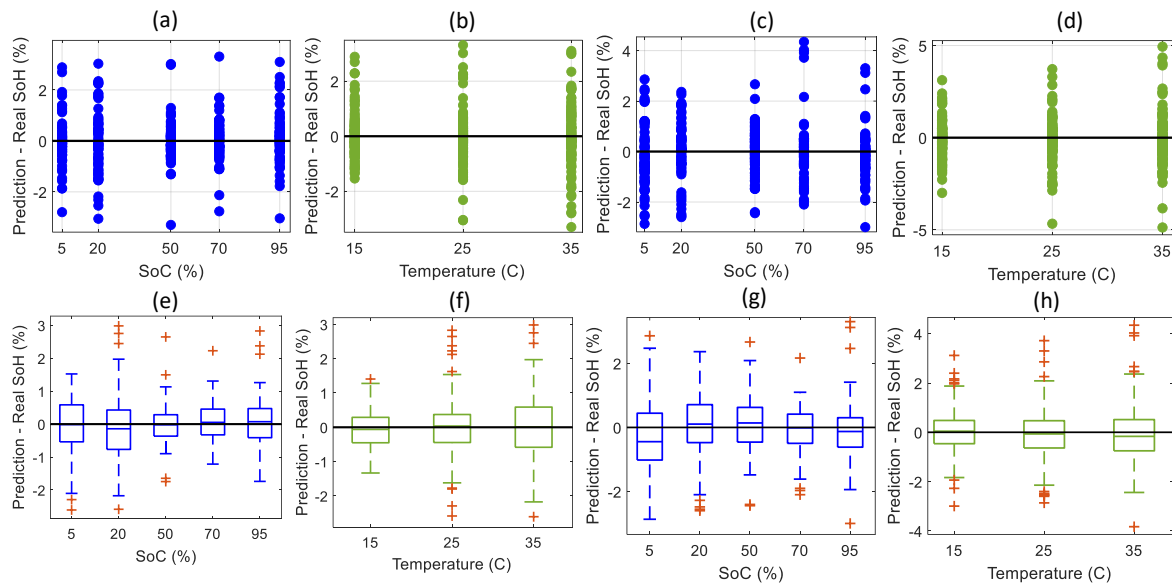
305 *Table 2. Accuracy metrics for predicting the cells SoH via the ML model*

Index Unit	RMSE (Mean) (%)	RMSE (Std) (%)	R ² (Mean) (-)	R ² (Std) (-)	MSE (Mean) (%)	MAE (Mean) (%)	Time (Mean) (sec)
Case Study 1	1.1096	0.0766	0.9759	0.0034	1.0374	0.6555	4011
Case Study 2	1.1397	0.0906	0.9750	0.0042	1.6407	0.8573	270

306 According to the table, the model with full data points, case study 1, has a higher accuracy, about
 307 0.03% better than the feature-based model, case study 2. This is also observable for the R² value which
 308 is about 0.01 better than the feature-based model. The difference between the two models become
 309 more visible in the MSE and the MAE and the time indices. The full data point model has a MSE of

310 0.6% and a MAE of 0.2% less than the feature-based model. However, the run time of the full point
 311 model is much more than that of the feature-based model which confirm the complexity of its training,
 312 according to the last column of the table the run time in case 1 is about 50 times higher than case 2.
 313 The run time has been calculated via a personal computer with 1.90 GHz and 2.11 GHz CPU and 16.0
 314 GB RAM. It is also worth noting that the standard deviation of the full point model is lower which
 315 implies that it is more stable than feature-based model.

316 To further highlight the performance of the model in different conditions, the distribution of the
 317 prediction error with respect to the conditioning features, (SoC and Temperature) is given in [Figure 8](#).
 318 Here the y axis refers the prediction versus real SoH value, as it is a subtraction of the predicted and
 319 real SoH in percent.



320 **Figure 8:** The distribution of prediction error at various conditions, (a) SoC case study 1, (b) temperature case
 321 study 1, (c) SoC case study 2, (d) temperature case study 2, (e) - (f) box plots case study 1, (g) - (h) box plots
 322 case study 2
 323

324 According to the [Figure 8](#), the distribution of the prediction error is quite different from one SoC point
 325 to another and from one temperature to another. The quantified errors are listed in [Table 3](#).

326 **Table 3.** Accuracy metrics for predicting the cells SoH via the ML model at various SoCs

Index	SoC (%)					Temperature (C)		
	5	20	50	70	95	15	25	35
Case Study 1								
Median	-0.0141	-0.1415	-0.0206	0.0533	0.0733	-0.0627	0.0358	0.0009
Lower Quartile	-0.5380	-0.7682	-0.3652	-0.3263	-0.4125	-0.4515	-0.4444	-0.5832
Higher Quartile	0.5852	0.4283	0.2854	0.4556	0.4726	0.2895	0.3725	0.5888
Case Study 2								
Median	-0.4446	0.1041	0.1395	-0.0122	-0.1269	0.0436	-0.0669	-0.1658
Lower Quartile	-1.0177	-0.4737	-0.4578	-0.4968	-0.6158	-0.4629	-0.6372	-0.7526
Higher Quartile	0.4439	0.7113	0.6251	0.4143	0.3031	0.4800	0.4699	0.5152

327 For case study 1, the largest prediction error median is 0.1415% at 20% SoC, [Figure 8 \(e\)](#), the median
 328 of error is largest at 15 °C, [Figure 8 \(f\)](#). For case study 2, the graphs of [Figure 8](#) and the indices on [Table](#)
 329 [3](#) show that the largest prediction error is related to the lowest SoC, (5%) with a median of 0.4446%.
 330 This error is minimum at mid-range SoC which is 70% with a median of 0.0122%. For temperature, the
 331 minimum prediction error is related to the room temperature (25 °C) with a median of 0.0669%, while
 332 the highest error is for highest temperature of 35 °C with a median of 0.1658 (%). It is also evident

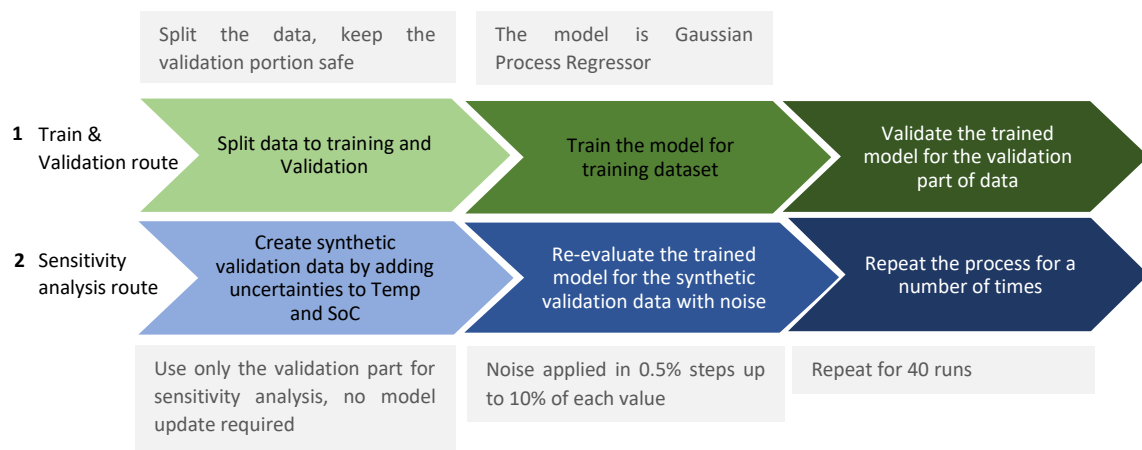
333 that the prediction error at a fixed SoC across all temperatures, [Figure 8 \(g\)](#), is having larger errors
 334 compared to the prediction at a particular temperature across all SoCs, [Figure 8 \(h\)](#). Summarising both
 335 case studies, it can be concluded that model performance is generally better at middle range SoC and
 336 temperatures. The implications of this for the future deployment of the model within a practical use
 337 case is explored further in the following section.

338 V. Discussions

339 V.I Sensitivity and robustness to noise

340 Understanding the source of measurement noise associated with making EIS measurements is
 341 particularly important during the development of the SoH estimation models by ML. The noise in the
 342 data is usually caused by the integrated components of the EIS measurement setups such as the
 343 connection cables and can be very misleading because of the slight excitation signals required for the
 344 EIS measurements [22]. Here the main source of noise is assumed to be originated from the SoC and
 345 Temperature measurements.

346 To evaluate the sensitivity of the developed SoH prediction model to noise, a noise analysis
 347 methodology is proposed here. The methodology is described in the [Figure 9](#).



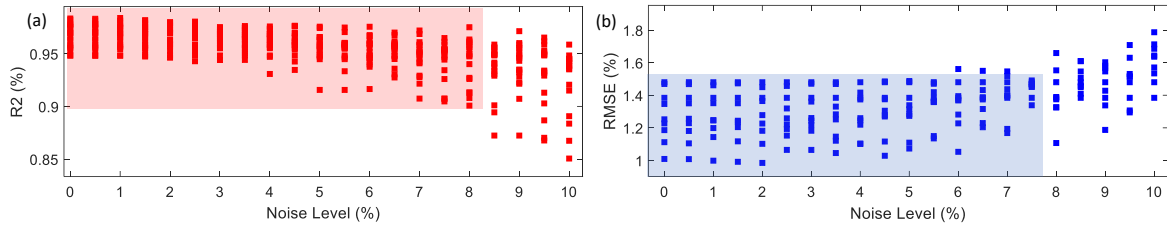
348

349 *Figure 9: The methodology to analyse the impact of the measurement noise on SoH prediction model's*
 350 *performance*

351 For this purpose, first the data is split into training and validation portions. The ratio of 80% for training
 352 and 20% for validation is preferred here. Then the model is trained on the training portion and
 353 validated on the remaining part. The validation portion is then altered by adding an uncertainty with
 354 the Gaussian distribution of mean zero and the standard deviation up to 10% of the temperature and
 355 SoC value at each record of data. This uncertainty is to represent the measurement noise for the two
 356 inputs synthetically. Then the model is validated against the new data without a change in its
 357 optimised hyperparameters. The whole process is repeated for multiple times to evaluate the
 358 repeatability of the method and increase the confidence in the results.

359 To capture the results, the models are iterated for 40 times to quantify the variation in the
 360 performance metrics and the impact of the random uncertainties. This number of repetitions is
 361 deemed suitable because of a balance between the stability of the results and the run time. The
 362 models start with a noise level of 0% and get evaluated by a stepwise increment in noise, 0.5% at each
 363 step, till 10% of the nominal value of the same record. The results at location 0 of x-axis contribute to
 364 the original data and the rest are based on synthetical noisy data. [Figure 10](#) implies that the model

370 can tolerate up to 8.2% of noise for an R^2 value higher than 90% and 7.8% of noise for a RMSE lower than 1.5%. Considering both metrics, an overlapping region is visible for up to 7.8% of measurement
 371 noise. The overlapping regions are visible in red and blue, respectively for the R^2 , Figure 10 (a), and
 372 RMSE, Figure 10 (b). The analysis confirms that the 7.8% of noise is still guaranteeing the model's
 373 performance to a good extent.

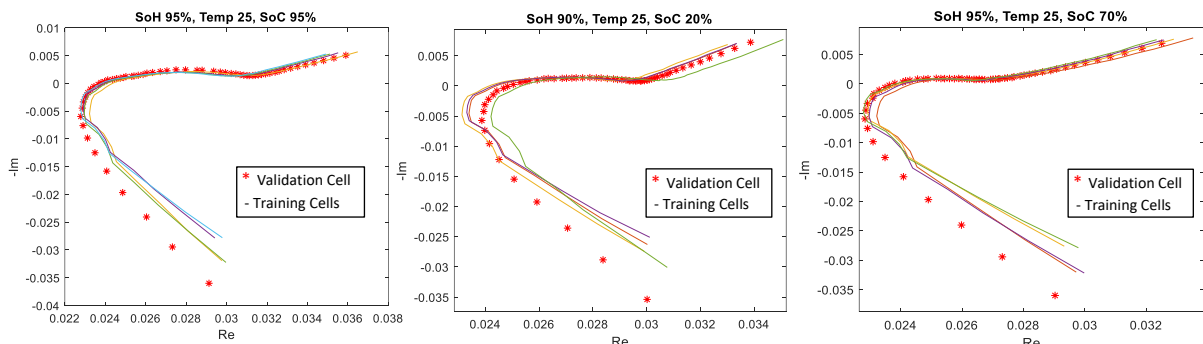


370
 371 **Figure 10:** The SoH prediction model sensitivity to measurement noise in temperature and SoC

372 **V.II Sensitivity and robustness to EIS characterisation equipment**

373 Although the EIS test profiles of the cell are mostly affected by the characterisations of the cell in
 374 terms of its SoH, SoC and temperature, the testing equipment and the experimental apparatus have
 375 also an undeniable impact on the EIS data features. In this section the trained model for which the
 376 data have been collected using the Multiplexer equipment, is validated against a new dataset that has
 377 been collected via an alternative equipment, Gamry which is a DC and impedance analyser. In the
 378 validation experiments, 5 cells were put under EIS test at 25 °C and a range of SoC conditions. Beside
 379 the difference in the testing equipment, their cooling mechanism was selected to be via turbulent air
 380 inside a thermal chamber rather than the oil cooling which was used during the collection of the first
 381 data set. Representing different levels of experimental fidelity and the possible impact this may have
 382 on model prediction performance. In total 25 experiments were conducted.

383 The testing equipment and the difference in the connections, cabling and cooling mechanism all had
 384 an impact on the cells EIS curve. This difference was quite obvious specially at the inductive tail of the
 385 EIS curves as shown in Figure 11.



386
 387 **Figure 11:** The impact of the testing equipment on the EIS measurements at different conditions (-) Multiplexer
 388 equipment (training data), (*) Gamry equipment (validation data)

389 **Table 4.** The performance of the model against the new EIS data with a different equipment

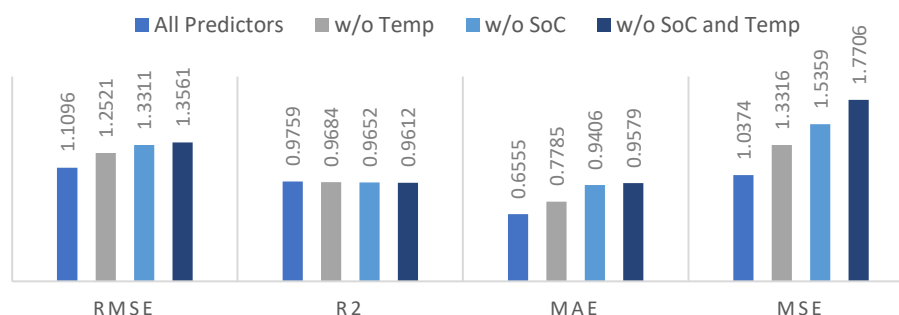
	Test Conditions			Model of Case Study 1		Model of Case Study 2	
	SoC	Temp	SoH (%)	Average Error (%)	RMSE (%)	Average Error (%)	RMSE (%)
Validation set 1	5-95%	25	89.4	2.86	1.38	3.61	1.62
Validation set 2	5-95%	25	95.0	-2.54	1.33	4.09	1.84
Validation set 3	5-95%	25	99.6	1.96	1.76	2.58	1.18
Validation set 4	5-95%	25	81.5	5.32	2.42	7.65	3.42
Validation set 5	5-95%	25	92.0	1.86	1.06	3.34	1.50

390 Considering the new data, Table 4 summarises the performance of the model in predicting the SoH of
 391 this new dataset while it is trained on the original data set. It is worth highlighting that the model has
 392 been completely blind to the new data during the training. Here, the Gamry equipment data are called
 393 the validation cell data for generality.

394 The results shown in Table 4, indicate that the methodology is reproducible. The model performs
 395 responds well to the change in the test equipment. Considering the model is trained by all the data
 396 points of the EIS curve, the average error of prediction for the 5 cases is 2.9%, while the RMSE is equal
 397 to 1.59%. Considering that the RMSE of the trained model via original dataset was actually 1.1096%
 398 these values are very much desirable. For the second model trained based on the features described
 399 in Table 1, the average prediction error for the 5 conditions is 4.25%, while the RMSE by average is
 400 1.91%. Comparing the feature-based and full point models reveals that the full-point model is more
 401 robust to the change in the testing equipment, which is believed to be due to its ability in
 402 generalisation because of the larger volume of information that it receives during training (61 data
 403 points) compared to the 7 data points of the feature-based configuration.

404 V.III SoC and Temperature contributions

405 The characterisation of second-life Lithium-ion batteries is a complex process which is affected by
 406 various factors such as the cells temperature, their SoC, their ageing history, the first life conditions as
 407 well as storage conditions. Measuring and quantifying all these factors is costly and non-practical
 408 specially when it comes to high volumes of cells and systems received from the provider. To realise
 409 the significance of each factor and its impact on the accuracy of the estimated SoH, an in-depth feature
 410 contribution analysis is crucial. In this section, the contribution of SoC and temperature on the
 411 predicted SoH accuracy is quantified. For this purpose, first the model is trained with all the predictors,
 412 which is SoC, temperature and all EIS datapoints, then various attempts have been made to train the
 413 model with a different set of predictors. A case involving only SoC and EIS data (without temperature),
 414 a case with temperature and EIS data (without SoC), and finally a case with only the EIS data (omitting
 415 SoC and Temperature) is created. A summary of the accuracy metrics of the models is provided at
 416 Figure 12. According to the comparative results, the model with full predictors has the best
 417 performance (lowest errors and highest R^2). Considering the model with all predictors as the baseline,
 418 it can easily be seen that removing the temperature from the predictor pool increases the prediction
 419 RMSE by about 12.84% and decreases the R^2 value by 0.77. A model without SoC increases the RMSE
 420 by 19.96% while reducing the R^2 by 1.09.



421
 422 *Figure 12. The impact of SoC and Temperature on the SoH prediction model performance*

423 A model without SoC and temperature leads to predictions with about 22.21% higher RMSE and circa
 424 1.50 lower R^2 which is the poorest performance. Considering the accuracy indices reported above, the
 425 temperature and SoC play an important role in the predictability of the SoH values. Comparing the

426 two cases that work without SoC or temperature as predictors, it is clear that SoC is a more
427 contributing factor to the accuracy of the model than temperature. This contribution analysis is crucial
428 when dealing with limitations regarding the measurements of SoC or temperature of cells for their
429 SoH estimation. In summary the SoC and temperature measurements are not necessary to be
430 obtained if the error levels of SoH prediction are considered tolerable or acceptable by the application
431 engineers during the characterisation process.

432 ***V.VI ML conflicts and limitations***

433 Generally, when it comes to the application of machine learning techniques for discoveries regarding
434 engineering problems, including those within the context of energy storage systems and Li-ion
435 batteries, three major challenges arise that need to be addressed reasonably to gain the confidence
436 of users. According to the literature and expert's view [52], these contradictions are about the three
437 following items. In this section is it explained how each item has been addressed in this study.

438 • *Data and Sample Size*

439 The second-life battery state of health is affected by a wide variety of factors such as its first life
440 conditions, storage conditions, its state of health, ageing mechanism and many more; however, it is
441 very costly and resource consuming to measurement and quantify all the mentioned factors. In a pilot
442 or laboratory scale characterisation line such as what is available in WMG, University of Warwick, it
443 has taken about 10 months to gather data for about 325 cases (for 35 cells). This time has been
444 invested to make sure that a reasonable volume of data is available to train the machine learning
445 models and make conclusions as general as possible. Furthermore, a second dataset is created for
446 validation purposes in a different testing condition than the original one used for model creation, and
447 a feature contribution analysis is performed to ease the decision making regarding the quantification
448 of less important variables for larger-scale experiments.

449 • *Complexity, Accuracy, and Ease of Use*

450 When it comes to the state of health estimation of Li-ion batteries, selecting the model configuration
451 and specially its hyperparameters are a major concern due to the nonlinear interconnections between
452 the factors and the response of cells. The strongest model if not tuned and optimised properly might
453 not be able to generalise the decisions from the training to the validation and test scenarios. In
454 general, linear models such as support vector machine with linear kernels, or simpler models such as
455 decision trees, although easy to train and use, usually have low accuracy and limited capability for
456 interpretability. Therefore, the application of more complex models is inevitable in this case. In this
457 study the GPR models are utilised to achieve a reasonable accuracy in balance with model training
458 complexities. For the maximum performance, Bayesian optimisation is utilised for the automatic
459 tuning of hyperparameters. The Bayesian optimisation technique while might be resource demanding
460 during the training process, is not raising a particular concern for this problem as the training of such
461 models usually take place in an offline configuration and only the model deployment which does not
462 have a specific resource requirement takes place in real-time.

463 • *Learning results and domain expert knowledge*

464 While ML models have been in wide use for the prediction of characteristics for lithium-ion related
465 problems, it is still a challenge to effectively include the prior knowledge of domain experts in models.
466 In this study, the authors have tried to incorporate this knowledge during the data collection, and

467 preparation stage of modelling and via expert-led feature engineering. It is worth mentioning that the
468 findings of this research were mostly in one of the two categories, 1) results that our experts had an
469 empirical prior expectation and understanding of those, and this research helped to quantify those,
470 such as the contribution of temperature and SoC to the SoH and their relative importance. 2) results
471 that were new to the experts such as the impact of measurement noise, testing conditions (EIS testing
472 equipment and cooling mechanism) on the response, which can initiate new lines of research for
473 future investigations. In general, it is acknowledged that creating a systematic approach for a weighted
474 and scored inclusion of expert knowledge is imperative, however, this requires extensive research and
475 it currently out of the scopes of our study.

476 VI. Conclusions

477 In this research, the prediction of the li-ion battery SoH using the EIS measurements and ML
478 approaches is addressed. This study is built upon a large number of experimental cases, 325 cases, by
479 taking into account the cell impedance across a desired range of frequencies between 10 mHz to 10
480 KHz, the effect of cell-to-cell variation, the cell state of charge, temperature, as well as characterisation
481 uncertainties. It links the SoH of cells to their EIS features at various experimental equipment
482 uncertainties and measurements noises. The methodology for creating the model beside the
483 approaches taken for uncertainty and robustness analysis are the main novelties of this study in the
484 context of Li-ion battery SoH estimation. Linking back to the research questions listed in the
485 introduction section, the following observations and findings can be summarised after this study.

- 486 • The EIS data beside the conditioning information can be directly used to predict the SoH of cells
487 with an accuracy up to 98.89%. Feature extraction and engineering can also be utilised for building
488 a ML model, in such case the accuracy drops to 98.86% which is still very desirable. This accuracy
489 reduction is due to the lost information when the EIS data are compressed from 61 frequency
490 points into only 7 features. If the training time is factored in, then the full EIS model is more
491 complex to be optimised with a training time of about 50 times higher than the feature-based
492 model. But and if the robustness of model is factored in, the full point model is more efficient than
493 the feature-based model (accuracy of 98.41% for new data set compared to 98.09%). Considering
494 the trade-off between accuracy, robustness, and the training effort, one model can be preferred
495 over the other one in a particular application. The accuracy obtained by either model implies that
496 the ML-based approaches can facilitate an accelerated SoH estimation method with a reasonable
497 effort.
- 498 • It is important that the model for SoH prediction be able to generalise the predictions from the
499 training data set to the new data sets. To provide this capability, considering a cross validation
500 approach during the training is necessary as it helps optimising the model's hyperparameters by
501 virtually creating a larger data set and considering each data point for validation at least once.
502 Testing the model's performance against a new dataset that was collected through a different
503 experimental equipment and under a different cooling mechanism showed that the ML model is
504 performing well with an error below 1.56% (case study 1) and 1.91% (case study 2). Further analysis
505 showed that model is also robust to the measurement noise of up to 7.8% of the nominal EIS
506 datapoints. This quantifies the level of noise that is tolerable when transferring the modelling
507 technology from one application to another where the quality of measuring equipment is not
508 necessarily the same.
- 509 • It is obvious that the SoH prediction accuracy depends on the information that is collected from
510 the cells for their impedance, temperature, and SoH. Considering the effort and resource required
511 for collecting this information, it is very valuable to be able to quantify each factor's impact on the

512 model accuracy. Through separating the impact of SoC and temperature on the model
513 performance, it was noted that the model is has its best performance with both features, and the
514 contribution of SoC to the model accuracy is higher than that of temperature. This means that in
515 case of resource limitation, the SoC characterisation should be prioritised to the temperature
516 measurements. It was also witnessed the model's performance is not the same across various SoC
517 and temperatures. According to the analysis, the ML model has the largest median of the prediction
518 error is at 20% SoC and 15 °C, which is believed to be due to the impact of other factors, such as
519 the type of again mechanisms, that have not taken into account or quantifies at low SoC or
520 temperatures.

521 The main future work planned in this research direction is about including further factors in cell
522 characterisation for its SoH estimation. Factoring in the cell's first life information, such as the charge
523 and discharge scenarios, the storage conditions and calender ageing is believed to enhance the model
524 accuracy. However, this requires an agreement between the cell providers after their first life and the
525 researchers in terms of data sharing and management. Another interesting direction for future studies
526 in the application of ML models and EIS tests for online estimation of SoH. In such case the
527 combination of the in-operando EIS test [21], and the proposed methodology for ML model creation
528 could be a fair solution.

529 **Supplementary Information**

530 The experimental data of this study will be available through a data in Brief Submission. Contact
531 Authors for further information.

532 **Acknowledgement**

533 This research was undertaken as part of the RECOVAS project, project funded by the UK Advanced
534 Propulsion Centre (APC), Grant Number: TS/V012789/1.

535 **Declaration of competing interest**

536 The authors declare that there is no known competing financial interests or personal relationships
537 that could have appeared to influence the work reported in this paper.

538 **CRediT**

539 Mona Faraji Niri: Conceptualization; Data curation; Formal analysis; Methodology; Software;
540 Visualization; Validation; Investigation; Writing - original draft. Muhammad Rashid: Methodology;
541 Data curation; Software; Investigation; Writing - original draft. Jonathan Sansom: Methodology;
542 Investigation; Writing - review & editing. Dhammika Widanage: Software, James Marco: Funding
543 acquisition; Supervision; Resources; Writing - review & editing.

544 **References**

545

- [1] A. Holland, J. Edmondson and L. Gear , "Lithium-ion Batteries for Electric Vehicles 2021-2031," IDTechEX, 2021.

- [2] Y. Jiang, J. Jiang, C. Zhang, W. Zhang and Y. Gao, "State of health estimation of second-life LiFePO₄ batteries for energy storage applications," *Journal of cleaner production*, vol. 205, pp. 754-762, 2018.
- [3] L. Ungurean, G. Cârstoiu, M. Micea and V. Groza, "Battery state of health estimation: a structured review of models, methods and commercial devices," *International Journal of Energy Research*, vol. 41, no. 2, pp. 151-181, 2017.
- [4] L. Yao, S. Xu, A. Tang, F. Zhou, J. Hou, Y. Xiao and Z. Fu, "A Review of Lithium-Ion Battery State of Health Estimation and Prediction Methods," *World Electric Vehicle Journal*, vol. 12, no. 3, p. 113, 2021.
- [5] M. Haram, J. Lee, G. Ramasamy, E. Ngu, S. Thiagarajah and Y. Lee, "Feasibility of utilising second life EV batteries: Applications, lifespan, economics, environmental impact, assessment, and challenges," *Alexandria Engineering Journal*, vol. 60, no. 5, pp. 4517-4536, 2021.
- [6] M. Abdel-Monem, O. Hegazy, N. Omar, K. Trad, P. Van den Bossche and J. Van Mierlo, "Lithium-ion batteries: Comprehensive technical analysis of second-life batteries for smart grid applications," in *19th European Conference on Power Electronics and Applications*, Warsaw, Poland, 2017.
- [7] E. Martinez-Laserna, E. Sarasketa-Zabala, I. Sarria, D. Stroe, M. Swierczynski, A. Warnecke, J. Timmermans, S. Goutam, N. Omar and P. Rodriguez, "Technical viability of battery second life: A study from the ageing perspective," *IEEE Transactions on Industry Applications*, vol. 54, no. 3, pp. 2703-2713, 2018.
- [8] A. Burke and M. Miller, "Life cycle testing of lithium batteries for fast charging and second-use applications," in *2013 World Electric Vehicle Symposium and Exhibition*, 2013.
- [9] S. Moura, N. Chaturvedi and M. Krstić, "Adaptive partial differential equation observer for battery state-of-charge/state-of-health estimation via an electrochemical model," *Journal of Dynamic Systems, Measurement, and Control*, vol. 136, no. 1, p. 011015, 2014.
- [10] Y. Gao, K. Liu, C. Zhu, X. Zhang and D. Zhang, "Co-estimation of state-of-charge and state-of-health for lithium-ion batteries using an enhanced electrochemical model," *IEEE Transactions on Industrial Electronics*, vol. 69, no. 3, pp. 2684-2696, 2021.
- [11] J. Li, K. Adewuyi, N. Lotfi, R. Landers and J. Park, "A single particle model with chemical/mechanical degradation physics for lithium ion battery State of Health (SOH) estimation," *Applied energy*, vol. 212, pp. 1178-1190, 2018.
- [12] Y. Li, M. Abdel-Monem, R. Gopalakrishnan, M. Bercibar, E. Nanini-Maury, N. Omar, P. van den Bossche and J. Van Mierlo, "A quick on-line state of health estimation method for Li-ion battery with incremental capacity curves processed by Gaussian filter," *Journal of Power Sources*, vol. 373, pp. 40-53, 2018.
- [13] M. Bercibar, M. Garmendia, I. Gandiaga, J. Crego and I. Villarreal, "State of health estimation algorithm of LiFePO₄ battery packs based on differential voltage curves for battery management system application," *Energy*, vol. 103, pp. 784-796, 2016.
- [14] C. Pastor-Fernández, K. Uddin and G. Chouchelamane, "A comparison between electrochemical impedance spectroscopy and incremental capacity-differential voltage as Li-ion diagnostic techniques to identify and quantify the effects of degradation modes within battery management systems," *Journal of Power Sources*, vol. 360, pp. 301-318, 2017.
- [15] D. Stroe, M. Swierczynski, A. Stan and V. Knap, "Diagnosis of lithium-ion batteries state-of-health based on electrochemical impedance spectroscopy technique," in *IEEE Energy Conversion Congress and Exposition*, 2014.

- [16] R. Mingant, J. Bernard, V. Moynot, A. Delaille, S. Mailley, J. Hognon and F. Huet, "EIS measurements for determining the SOC and SOH of Li-ion batteries," *ECS Transactions*, vol. 33, no. 39, p. 41, 2011.
- [17] J. Kim, L. Krüger and J. Kowal, "On-line state-of-health estimation of Lithium-ion battery cells using frequency excitation," *Journal of Energy Storage*, vol. 32, p. 101841, 2020.
- [18] R. Mingant, J. Bernard and V. Sauvant-Moynot, "Novel state-of-health diagnostic method for Li-ion battery in service," *Applied Energy*, vol. 183, pp. 390-398, 2016.
- [19] M. Messing, T. Shoa and S. Habibi, "Estimating battery state of health using electrochemical impedance spectroscopy and the relaxation effect," *Journal of Energy Storage*, vol. 43, p. 103210, 2021.
- [20] C. Pastor-Fernández, W. Widanage, J. Marco, M. Gama-Valdez and G. Chouchelamane, "Identification and quantification of ageing mechanisms in Lithium-ion batteries using the EIS technique," in *IEEE Transportation Electrification Conference and Expo*, Dearborn, MI, 2016.
- [21] N. Hallems, W. Widanage, X. Zhu, S. Moharana, M. Rashid, A. Hubin and J. Lataire, "Operando electrochemical impedance spectroscopy and its application to commercial Li-ion batteries," *Journal of Power Sources*, vol. 547, p. 232005, 2022.
- [22] Y. Xing, E. Ma, K. Tsui and M. Pecht, "An ensemble model for predicting the remaining useful performance of lithium-ion batteries," *Microelectronics Reliability*, vol. 53, no. 6, pp. 811-820, 2013.
- [23] L. Chen, H. Wang, B. Liu, Y. Wang, Y. Ding and H. Pan, "Battery state-of-health estimation based on a metabolic extreme learning machine combining degradation state model and error compensation," *Energy*, vol. 215, p. 119078, 2021.
- [24] H. Pan, Z. Lü, H. Wang, H. Wei and L. Chen, "Novel battery state-of-health online estimation method using multiple health indicators and an extreme learning machine," *Energy*, vol. 160, pp. 466-477, 2018.
- [25] R. Li, J. Hong, H. Zhang and X. Chen, "Data-driven battery state of health estimation based on interval capacity for real-world electric vehicles," *Energy*, vol. In press, p. 124771, 2022.
- [26] Y. Che, Z. Deng, P. Li, X. Tang, K. Khosravinia, X. Lin and X. Hu, "State of health prognostics for series battery packs: A universal deep learning method," *Energy*, vol. 238, p. 121857, 2022.
- [27] M. Alipour, S. Tavallaey, A. Andersson and D. Brandell, "Improved Battery Cycle Life Prediction Using a Hybrid Data-Driven Model Incorporating Linear Support Vector Regression and Gaussian," *ChemPhysChem*, vol. 23, no. 7, p. e202100829, 2022.
- [28] H. Goh, Z. Lan, D. Zhang, W. Dai, T. Kurniawan, and K. Goh, "Estimation of the state of health (SOH) of batteries using discrete curvature feature extraction," *Journal of Energy Storage*, vol. 50, p. 104646, 2022.
- [29] Y. Gong, X. Zhang, D. Gao, H. Li, L. Yan, J. Peng and Z. Huang, "State-of-health estimation of lithium-ion batteries based on improved long short-term memory algorithm," *Journal of Energy Storage*, vol. 53, p. 105046, 2022.
- [30] Z. Xia and J. Qahouq, "Evaluation of parameter variations of equivalent circuit model of lithium-ion battery under different SOH conditions," in *IEEE Energy Conversion Congress and Exposition*, Detroit, MI, USA, 2020.
- [31] A. Zenati, P. Desprez and H. Razik, "Zenati, A., Desprez, P. and Razik, H., 2010, November. Estimation of the SOC and the SOH of li-ion batteries, by combining impedance measurements with the fuzzy logic inference," in *36th Annual Conference on IEEE Industrial Electronics Society*, 1773-1778, 2010.

- [32] Y. Zhang, Q. Tang, Y. Zhang, J. Wang, U. Stimming and A. Lee, "Identifying degradation patterns of lithium ion batteries from impedance spectroscopy using machine learning," *Nature communications*, vol. 11, no. 1, pp. 1-6, 2020.
- [33] W. Li, J. Chen, K. Quade, D. Luder, J. Gong and D. U. Sauer, "Battery degradation diagnosis with field data, impedance-based modeling and artificial intelligence," *Energy Storage Materials*, vol. 53, pp. 391-403, 2022.
- [34] Y. Li, B. Dong, T. Zerrin, E. Jauregui, X. Wang, X. Hua, D. Ravichandran, R. Shang, J. Xie, M. Ozkan and C. Ozkan, "State-of-health prediction for lithium-ion batteries via electrochemical impedance spectroscopy and artificial neural networks," *Energy Storage*, vol. 2, no. 5, p. 186, 2020.
- [35] Z. Xia and J. Qahouq, "Adaptive and fast state of health estimation method for lithium-ion batteries using online complex impedance and artificial neural network," in *IEEE Applied Power Electronics Conference and Exposition*, Anaheim, CA, USA, 2019.
- [36] Y. Zhang, Q. Tang, Y. Zhang, J. Wang, U. Stimming and A. Lee, "Identifying degradation patterns of lithium ion batteries from impedance spectroscopy using machine learning," *Nature communications*, vol. 11, no. 1, pp. 1-6, 2020.
- [37] I. Babaeiyazdi, A. Rezaei-Zare and S. Shokrzadeh, "State of charge prediction of EV Li-ion batteries using EIS: A machine learning approach," *Energy*, vol. 223, p. 120116, 2021.
- [38] A. Densmore and M. Hanif, "Determining battery SoC using electrochemical impedance spectroscopy and the extreme learning machine," in *2nd International Future Energy Electronics Conference*, Taipei, Taiwan, 2015.
- [39] Y. Jiang, J. Jiang, C. Zhang, W. Zhang and Y. Gao, "Recognition of battery aging variations for LiFePO₄ batteries in 2nd use applications combining incremental capacity analysis and statistical approaches," *Journal of Power Sources*, vol. 360, pp. 180-188, 2017.
- [40] M. Rashid and A. Gupta, "Effect of Relaxation Periods over Cycling Performance of a Li-Ion Battery," *Journal of The Electrochemical Society*, vol. 162, no. 2), pp. A3145-A3153, 2015.
- [41] A. Barai, G. Chouchelamane, Y. Guo, A. McGordon and P. Jennings, "A study on the impact of lithium-ion cell relaxation on electrochemical impedance spectroscopy," *Journal of Power Sources*, vol. 280, pp. 74-80, 2015.
- [42] C. Rasmussen and H. Nickisch, "Gaussian processes for machine learning (GPML) toolbox," *Journal of Machine Learning Research*, vol. 11, pp. 3011-3015, 2010.
- [43] K. Liu, X. Hu, Z. Wei, Y. Li and Y. Jiang, "Modified Gaussian process regression models for cyclic capacity prediction of lithium-ion batteries," *IEEE Transactions on Transportation Electrification*, vol. 5, no. 4, pp. 1225-1236, 2019.
- [44] R. Richardson, C. Birkl, M. Osborne and D. Howey, "Gaussian process regression for in situ capacity estimation of lithium-ion batteries," *IEEE Transactions on Industrial Informatics*, vol. 15, no. 1, pp. 127-138, 2018.
- [45] D. Yang, X. Zhang, R. Pan, Y. Wang and Z. Chen, "A novel Gaussian process regression model for state-of-health estimation of lithium-ion battery using charging curve," *Journal of Power Sources*, vol. 384, pp. 387-395, 2018.

- [46] T. Fushiki, "Estimation of prediction error by using K-fold cross-validation," *Statistics and Computing*, vol. 21, no. 2, pp. 137-146, 2011.
- [47] B. Liaw and G. Pistoia, *Behaviour of Lithium-Ion batteries in electric vehicles*, Berlin, Germany: Springer International Publishing, 2018.
- [48] C. Pastor-Fernandez, T. F. Yu, W. D. Widanage and J. Marco, "Critical review of non-invasive diagnosis techniques for quantification of degradation modes in lithium-ion batteries," *Renewable and Sustainable Energy Reviews*, vol. 109, pp. 138-159, 2019.
- [49] A. Bizeray, J. Kim, S. Duncan and D. Howey, "Identifiability and parameter estimation of the single particle lithium-ion battery model," *IEEE Transactions on Control Systems Technology*, vol. 27, no. 5, pp. 1862-1877, 2018.
- [50] E. Komaroff, "Relationships Between p-values and Pearson Correlation Coefficients, Type 1 Errors and Effect Size Errors, Under a True Null Hypothesis," *Journal of Statistical Theory and Practice*, vol. 14, no. 3, pp. 1-13, 2020.
- [51] N. Gogtay and U. Thatte, "Principles of correlation analysis," *Journal of the Association of Physicians of India*, vol. 65, no. 3, pp. 78-81, 2017.
- [52] Y. Liu, B. Guo, X. Zou, Y. Li and S. Shi, "Machine learning assisted materials design and discovery for rechargeable batteries," *Energy Storage Materials*, vol. 31, pp. 434-450, 2020.
- [53] J. Benesty, J. Chen, Y. Huang and I. Cohen, "Pearson Correlation Coefficient," in *Noise Reduction in Speech Processing*. Springer Topics in Signal Processing, Berlin, Heidelberg, Springer, 2009.

546

547